Journal of
Materials Chemistry C

ROYAL SOCIETY
OF CHEMISTRY

PAPER

View Article Online
View Journal | View Issue

Cite this: *J. Mater. Chem. C*, 2024, **12**, 11521

Carbon–$Ni_6Co_3Fe_1$ alloy hybrid foil for electromagnetic wave interference shielding in X-band and extremely low frequencies†

Jihun Lee,‡[a] Yun Seong Cho,‡[a] Dongjoon Rhee,‡[ab] Hakjeong Kim,[c] Sera Jeon,[d] Dohyun Lee,[a] Jae Won Heo,[aef] Moosung Choi,[g] Ji Hoon Seo,[g] Joon-Young Soh,[g] In Soo Kim,[aef] Sang-Woo Kim,*[d] Dukhyun Choi*[chi] and Joohoon Kang*[aef]

Received 22nd June 2024,
Accepted 27th June 2024

DOI: 10.1039/d4tc02611j

rsc.li/materials-c

Carbon-based materials, such as graphite foil, are widely recognized as excellent electromagnetic interference shielding materials due to their outstanding electrical conductivity, lightweight nature, and chemical inertness. While these materials serve as effective shields at high frequencies, their shielding performance for electromagnetic waves in the extremely low frequency regime is significantly diminished. In this manuscript, we propose an approach to fabricate carbon-based shielding materials that can be applied over the multiple electromagnetic spectral regions. By electrochemically depositing nickel, cobalt, and iron (NiCoFe) alloy film onto a graphite foil, we achieved a shielding composite covering extremely low and X-band frequencies. The nanostructured NiCoFe alloy film with excellent electrical and magnetic properties enhanced shielding effectiveness in the high-frequency regime by reflection and absorption, whereas extremely-low-frequency magnetic fields were effectively shielded through magnetic flux-shunting mechanisms. The enhanced shielding performance of the NiCoFe/graphite foil was also accompanied by improved thermal and mechanical properties. As our process is facile and scalable, we anticipate that this composite shielding strategy will potentially serve as a promising solution for practical electromagnetic interference shielding applications.

Introduction

The ever-expanding usage of electronics and communication technology has filled our daily lives with electromagnetic (EM) radiations from diverse sources, including mobile phones, personal computers, and televisions, the internet, wireless networks, and aerospace communication technologies. In particular, the number of wireless local area network (WLAN)-connected devices in major cities worldwide has more than doubled between 2016 and 2021, highlighting the increasing pace of technological development and the expanding range of applications.[1] Shielding against electromagnetic interference (EMI) is therefore increasingly important to ensure the stable operation of devices without malfunctioning and to guarantee reliable transmission and reception of information for wireless communication.[2] Furthermore, EMI shielding is also crucial for minimizing the potential hazards to human health because prolonged exposure to EM radiations can result in various health issues including cancer, sleep disorders, cognitive abnormalities, and cardiovascular diseases.[3–5]

The ability of a material to shield against EMI is evaluated by the shielding effectiveness (SE_T), which is defined as the logarithmic ratio of the powers (P), or the intensities of the electric (E) and magnetic (H) fields, of the incident and transmitted EM waves expressed in decibels.[6]

$$SE_T = 10\log(P_i/P_t) = 20\log|E_i/E_t| = 20\log|H_i/H_t| \qquad (1)$$

where subscripts i and t denote the incident and transmitted EM waves. In general, the EMI shielding by a material is

---

[a] *School of Advanced Materials Science and Engineering, Sungkyunkwan University (SKKU), Suwon 16419, Republic of Korea. E-mail: joohoon@skku.edu*
[b] *Department of Electrical and Systems Engineering, University of Pennsylvania, Philadelphia, PA, USA*
[c] *School of Mechanical Engineering, Sungkyunkwan University, Suwon 16419, Republic of Korea. E-mail: bred96@skku.edu*
[d] *Department of Materials Science and Engineering, Yonsei University, Seoul 03722, Republic of Korea. E-mail: kimsw1@yonsei.ac.kr*
[e] *The Nanophotonics Research Center, Korea Institute of Science and Technology (KIST), Seoul 02792, Republic of Korea*
[f] *KIST-SKKU Carbon-Neutral Research Center, Sungkyunkwan University, Suwon 16419, Republic of Korea*
[g] *Korea Electric Power Research Institute, 34056 Daejeon, Republic of Korea*
[h] *Department of Future Energy Engineering, Sungkyunkwan University, Suwon 16419, Republic of Korea*
[i] *SKKU Institute of Energy Science & Technology (SIEST), Sungkyunkwan University, Suwon 16419, Republic of Korea*

† Electronic supplementary information (ESI) available. See DOI: **https://doi.org/10.1039/d4tc02611j**

‡ Jihun Lee, Yun Seong Cho, and Dongjoon Rhee contributed equally.

achieved by contribution from three loss mechanisms: (1) reflection (SE_R), (2) absorption (SE_A), and (3) multiple reflections (SE_M)

$$SE_T = SE_R + SE_A + SE_M \qquad (2)$$

where the multiple reflection term is typically negligible when the thickness of the shield is larger than the skin depth or when $SE_T > 15$ dB.[7,8] The reflection loss occurs because part of the incident EM wave is reflected by the response of free electrons at the shield surface. For a plane EM wave, whose electric and magnetic fields perpendicular to each other and related by the intrinsic impedance of the medium, the reflection loss scales with the mismatch between the impedance of free space ($\eta_0 = \sqrt{\mu_0/\varepsilon_0} \approx 377\Omega$, where are ε_0 and μ_0 permittivity and permeability of free space) and the impedance of the shield (η).[9] For a conductive shield ($\eta \ll \eta_0$), the reflection loss can be described by the following equation.[6]

$$SE_R = 20\log\frac{(\eta+\eta_0)^2}{4\eta\eta_0} \approx 20\log\frac{\eta_0}{4\eta} = 39.5 + 10\log\frac{\sigma}{2\pi f\mu} \qquad (3)$$

where f is the frequency of the EM wave, and σ and μ are the electrical conductivity and magnetic permeability of the shield, respectively.[6] The portion of the EM wave passing through the shield is attenuated by various mechanisms, including ohmic losses from induced currents, interactions between the EM wave and electric/magnetic dipoles, as well as losses from magnetic hysteresis and eddy currents.[6,10] As a result, the field intensity exponentially decays with a characteristic attenuation coefficient (α) and thus the absorption loss is expressed by the following equation for a shielding material with a thickness of t.

$$SE_A = 20\log e^{\alpha t} = 8.68t\sqrt{\pi f\mu\sigma} \qquad (4)$$

The most common sources of electromagnetic pollution in daily life are radio frequency EM waves with frequencies ranging from tens of megahertz (MHz) to tens of gigahertz (GHz), which are used for FM radio, mobile phones, wireless network, microwave ovens, and radar. In this frequency regime, the traveling EM wave can mostly be considered as a uniform plane wave since the near-field region only extends several centimeters to meters from the source, and the wave impedance (Z_w, defined as E/H) is equal to the impedance of free space ($Z_w = \eta_0 \approx 377\ \Omega$).[9] Therefore, materials with high electrical conductivities (small η) are typically the most effective shielding materials for MHz- and GHz-frequency EM waves owing to their large impedance mismatch with free space that leads to high SE_R (eqn (3)), along with high SE_A for ohmic loss (eqn (4)).[11–15] Metals such as aluminum and copper are conventionally used as EMI shielding materials due to their high electrical conductivities, but they are susceptible to corrosion and are relatively heavy.[16] Carbon-based materials, including carbon nanotubes, graphite, and graphene, have been widely investigated as alternative EMI shielding materials due to their excellent electrical properties, corrosion resistance, lightweight nature, and mechanical flexibility.[17–20] With electrical conductivities ranging from 10^4 to 10^8 S m^{-1}, EMI shields based on these carbon materials have demonstrated excellent shielding effectiveness across wide frequency ranges, including the X-band (8.2–12.4 GHz), commonly employed in radar, satellite communication, and wireless computer networks.[17]

Joohoon Kang

Prof. Joohoon Kang is an Assistant Professor in the School of Advanced Materials Science and Engineering and the KIST-SKKU Carbon Neutral Research Center at Sungkyunkwan University (SKKU). He received his BS and MS degrees in materials science and engineering from Yonsei University in Korea in 2009 and 2011, respectively, and his PhD degree in materials science and engineering from Northwestern University in 2018. He then moved to the University of California at Berkeley as a postdoctoral fellow in the College of Chemistry. His research interests include synthesis, processing, and (opto)electronic applications of nanomaterials.

While conductive materials are effective in shielding high-frequency EM waves through reflection and absorption, shielding against extremely low-frequency EM waves (1–300 Hz) from magnetic field sources is challenging regardless of the thickness of the conductive shield. In this frequency regime, the near field region extends up to 1000–100 000 kilometres from the source, resulting in the EM wave behaving differently from a plane wave in most situations. Within the near-field region, the EM wave exhibits predominance of either electric or magnetic fields, and its wave impedance deviates from the characteristic impedance of free space.[9,21] Extremely low-frequency EM waves from an electric field source ($Z_w > \eta_0$) exhibit a higher impedance mismatch with the shielding material compared to plane EM waves, enabling effective shielding through the reflection mechanism. In contrast, the reflection loss for EM waves from a magnetic field source ($Z_w < \eta_0$) is negligible due to their low impedance, especially at low frequencies ($SE_R \propto \log(f)$).[6] The mechanisms responsible for the EM wave absorption (*e.g.* ohmic losses from induced currents and eddy current losses) are also marginal in the extremely low-frequency regime, resulting in minor absorption losses ($SE_A \propto f^{1/2}$).[6] As a result, an alternative approach is necessary to shield magnetic-field-dominated EM waves with extremely low frequencies. One such method is to divert the magnetic flux using materials with high magnetic permeability.[22] Because the highly permeable shield has a much lower reluctance than free space, the magnetic field and flux will concentrate within the shield, effectively protecting the region of interest against magnetic field. Ferromagnetic metals such as iron (Fe), nickel (Ni), and cobalt (Co) are representative examples of high permeability materials that can be used for shielding extremely low-frequency EM waves from magnetic field sources, but less effective in shielding high-frequency EM waves.[23] Combining highly conductive materials with these ferromagnetic metals in the form of composites would enable high EMI shielding performance across both high and low frequency regimes. However, ensuring the optimal performance of each component, as well as achieving the mechanical integrity, remains challenging.

Herein, we report an EM shielding foil by integrating magnetically permeable NiCoFe ternary alloy films onto electrically conductive graphite foils through a facile electrochemical deposition process. The NiCoFe/graphite composite shield achieved excellent EMI shielding effectiveness in the X-band, with the reflection and absorption losses higher than graphite due to its higher electrical conductivity. Additionally, benefiting from the magnetic properties of the NiCoFe layer, the composite shield can also shield against magnetic-field-dominant EM wave in the ELF regime, thereby demonstrating effective shielding behavior over multiple spectral regions. The electrical and magnetic properties of the NiCoFe/graphite composite and individual components were characterized and compared to confirm the benefits of the alloy for improved shielding performance in different frequency regimes. Finally, the NiCoFe/graphite foil exhibited enhanced thermal and mechanical properties, highlighting the advantages of our strategy for practical applications.

Results and discussion

Fabrication of NiCoFe/graphite composite EMI shield

EM waves can be categorized based on their frequency into various groups, including microwave, radio wave, low frequency, and extremely low frequency (ELF) (Fig. 1a). Depending on the frequency, different shielding strategies are needed to protect a region from EM waves. For high-frequency EM waves such as microwaves, materials with high electrical conductivities are effective for EMI shielding, primarily through reflection with the assistance of absorption (Fig. 1b).[24,25] On the other hand, ELF waves from magnetic field sources mostly penetrate these conventional shielding materials with minimal reflection and absorption, which necessitates shields with high magnetic permeability to divert the EM wave from the region of interest based on magnetic field-shunting effects (Fig. 1c).[26,27] To effectively shield against both high-frequency and ELF EM waves, we have designed a EMI shielding material by integrating the graphite foil, which is characterized by excellent electrical properties (high frequency shielding), and NiCoFe alloy film, which has excellent magnetic properties (ELF shielding).

Fig. 2a depicts the process to form NiCoFe alloy films on graphite foils using an electrochemical cell with an electrolyte solution containing shielding metal ions and saccharin (Experimental section in ESI†). When a potential was applied, shielding metal ions were deposited onto the graphite foil acting as the working electrode. The inclusion of saccharin in the electrolyte facilitated the formation of fine-grained NiCoFe deposits.[28–30] To ensure simultaneous reduction of Ni^{2+}, Co^{2+}, and Fe^{2+} ions essential for the uniform alloy formation and to achieve a high deposition rate, we applied a constant DC voltage (4.5 V) much higher than the standard reduction potentials of these elements (−0.25 V, −0.28 V, and −0.44 V for Ni^{2+}, Co^{2+}, and Fe^{2+}, respectively),[31] resulting in a current density ranging from -18 mA cm^{-2} to -19 mA cm^{-2} (Fig. S1, ESI†). In addition, applying a high voltage increases the deposition rate and thus

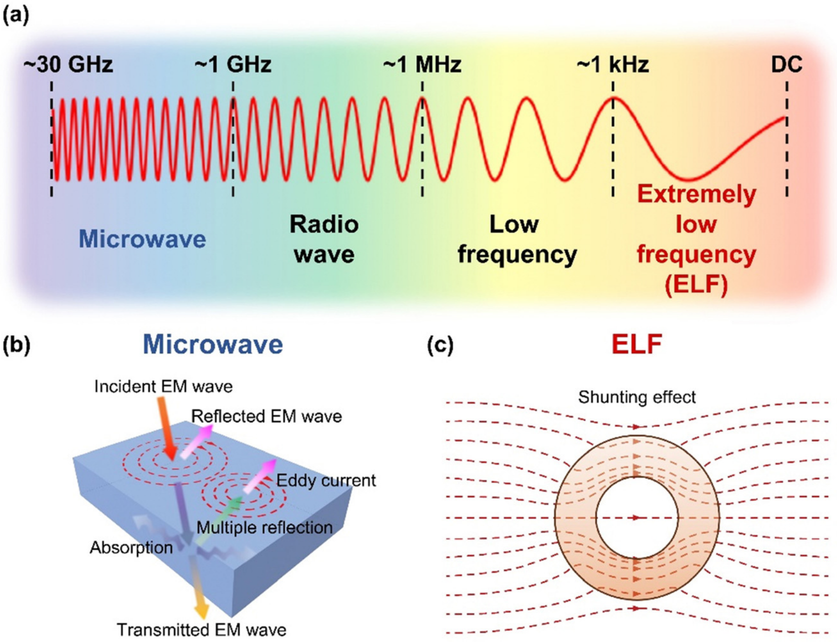

Fig. 1 EMI shielding strategies for different frequency ranges. (a) Classification of the electromagnetic spectrum by frequency. (b) Conventional approach for shielding against EM waves through reflection, absorption, and multiple reflections, which is commonly used for microwave shielding. (c) Strategy for shielding against magnetic-field-dominated EM waves with extremely low frequencies through the magnetic flux-shunting mechanism.

creates more nucleation sites for the formation of smaller grain sizes, which can enhance the mechanical properties of the resulting composite.[32] The successful deposition of the NiCoFe film was visually confirmed by the presence of silver-colored region in the photograph of the graphite foil after the electrochemical process (Fig. 2b). Based on the scanning electron microscope (SEM) images of the electrochemically deposited area on the graphite foil, we observed that the NiCoFe film exhibited a fine-grained and uniform film structure (Fig. S2, ESI†). The film thickness was ∼7 μm after 30 minutes of electrochemical deposition and increased to ∼18 μm after 3 hours, as deduced from the cross-sectional SEM images (Fig. S3, ESI†). To further analyze the structure and composition in detail, transmission electron microscope (TEM) images of the NiCoFe film surface were analyzed (Fig. 2c). The image revealed that grains at the scale of tens of nanometers were uniformly distributed across the film. Additionally, the film was characterized with energy-dispersive X-ray spectroscopy (EDS) mapping to analyze the elemental composition of the electrochemically deposited NiCoFe film. Over the region examined in Fig. 2d, the distribution of Co, Ni and Fe atoms was uniform, indicating the formation of alloy. The elemental ratio of the NiCoFe alloy film was determined to be Ni : Co : Fe = 6 : 3 : 1 based on EDS spectra (Fig. S4 and Table S1, ESI†). We also performed X-ray diffraction (XRD) analysis to elucidate the crystallinity of the NiCoFe/graphite sample (Fig. 2e). In addition to peaks from the graphite foil substrate (2θ = 26.7° and 54.8°), characteristic peaks associated with the NiCoFe ternary alloy were observed at 2θ = 44.4° and 51.3°. These peaks correspond to the (111) and (200) planes of the face-centered cubic (FCC) Co and Ni, indicating that the NiCoFe alloy forms an FCC crystal structure. Notably, we did not observe peaks related to the body-centered cubic (BCC) arrangement of Fe, which is the stable crystal structure of Fe at room temperature. The absence of peaks related to BCC Fe suggests that the all three elements are intermixed and form a homogeneous FCC phase.[33] The FCC structure of the NiCoFe alloy was further confirmed by high-resolution TEM images. In particular, in the region shown in Fig. 2f inset, the (110) surface of the FCC structure was clearly identified with the measured interplanar spacing of the (111) planes (d_{111}) to be 2.14 Å. This interplanar spacing corresponds to the FCC lattice of Ni, indicating that the crystal structure of our NiCoFe alloy film follows that of Ni, which was the most abundant among the three constituent elements. As expected from the low-resolution TEM image (Fig. 2c), the selected area electron diffraction (SAED) pattern showed ring patterns corresponding to d_{111} =2.14 Å, further revealing that the film is polycrystalline and comprises of fine grains with the FCC crystal structure. To analyze

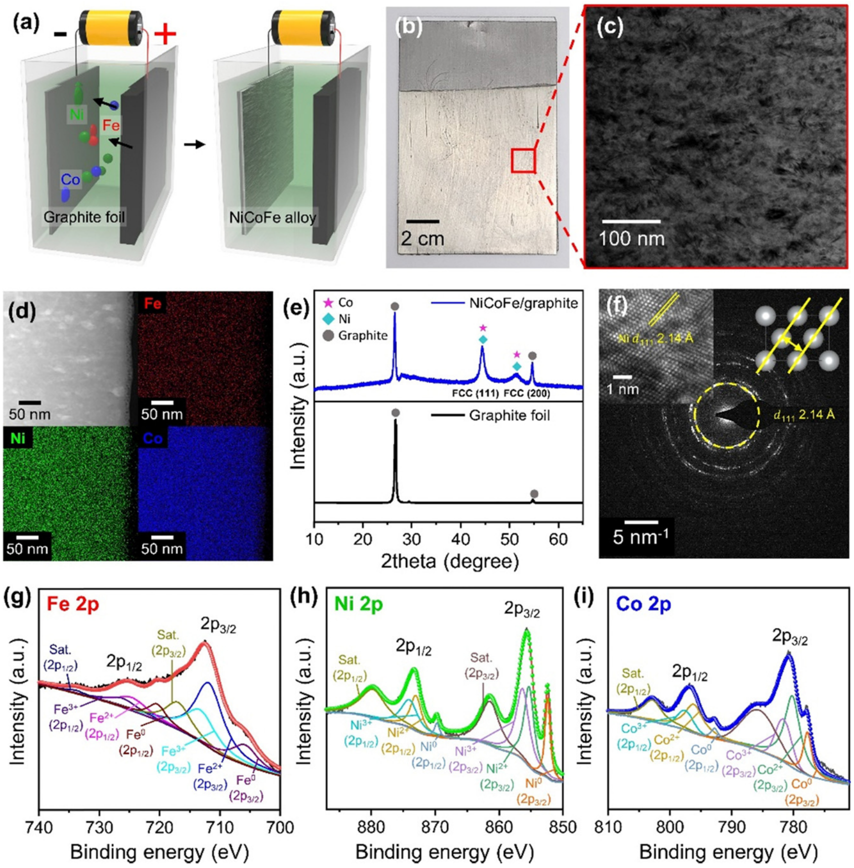

Fig. 2 Fabrication of NiCoFe/graphite composite EMI shield through electrochemical deposition. (a) Schematic illustration of the electrochemical deposition process for creating NiCoFe alloy films on graphite foils. (b) and (c) Photograph and TEM image of the fabricated NiCoFe/graphite composite EMI shield. (d) EDS elemental mapping of the NiCoFe alloy film obtained using TEM. (f) XRD patterns of graphite and NiCoFe/graphite foils. (e) HRTEM image and SAED pattern of the NiCoFe alloy film. (g)–(i) Core-level XPS spectra of the NiCoFe alloy film: (g) Fe 2p, (h) Ni 2p, and (i) Co 2p.

the bonding interactions among the constituent elements in the NiCoFe ternary alloy, the NiCoFe/graphite foil was characterized with X-ray photoelectron spectroscopy (XPS) (Fig. 2g–i). In the Fe 2p core-level XPS spectrum, two main $2p_{3/2}$ and $2p_{1/2}$ peaks corresponding to Fe^{2+} (712.1 eV and 724.9 eV) and Fe^{3+} (713.8 eV and 726.3 eV) were observed, along with satellite peaks (717.2 eV and 734.2 eV) and Fe^0 peaks (705.6 eV and 720.2 eV). Similar observations were found in Ni 2p and Co 2p core-level XPS spectra. In the case of Ni, main peaks corresponding to Ni^{2+} (855.4 eV and 873.1 eV) and Ni^{3+} (856.4 eV and 874.1 eV) were identified, as well as satellite peaks (861.6 eV and 880.1 eV) and Ni^0 peaks (852.5 eV and 869.6 eV). Similarly, for Co, Co^{2+} (780.3 eV and 796.3 eV) and Co^{3+} (781.7 eV and 797.7 eV) were observed, accompanied by satellite peaks (785.5 eV and 802.8 eV) and Co^0 peaks (777.8 eV and 792.8 eV). The peaks corresponding to the zero-valent states (Fe^0, Ni^0, Co^0) can be attributed to the Ni, Co, and Fe atoms uniformly alloyed with each other to form a single phase,[34] while the oxidation state peaks are associated with surface oxidation that commonly occurs during sample preparation and exposure to ambient air.[35]

EMI shielding effect of NiCoFe/graphite foil

As the electrical conductivity of the shield is an important factor in determining the shielding effectiveness for high-frequency EM waves, we first investigated the electrical properties of the NiCoFe/graphite composite based on the sheet resistance (Fig. 3a). We also characterized the graphite foil and free-standing NiCoFe alloy film to measure the electrical properties of each component (Experimental section in ESI†). The sheet resistance of graphite foil was measured to be 60.9 mΩ sq^{-1}. The free-standing NiCoFe alloy film exhibited a sheet resistance of 34.4 mΩ sq^{-1}, which suggests that the NiCoFe alloy was more conductive than graphite. In the case of the NiCoFe/graphite composite, the sheet resistance (33.4 mΩ sq^{-1}) was nearly the same as the free-standing NiCoFe film because the surfaces consisted of the same NiCoFe alloy. The comparison of sheet resistance among samples indicates the excellent electrical conductivity of the electrochemically deposited NiCoFe alloy and suggests additional synergistic shielding effects with the graphite foil.

We then evaluated the EMI shielding effectiveness of the samples in the high-frequency range, focusing on the X-band as a representative region of high-frequency EM waves. Fig. 3b–d show the total shielding effectiveness (SE_T), along with the absorption loss (SE_A) and reflection loss (SE_R), determined based on the scattering parameters measured by a vector network analyzer (Experimental section in ESI†). Graphite exhibited a slightly higher shielding effectiveness (SE_T) with an average value of 54.50 dB in the X-band than the free-standing NiCoFe alloy film (average SE_T of 50.42 dB) (Fig. 3b). Interestingly, the NiCoFe/graphite composite showed a notably higher average shielding effectiveness of 68.90 dB compared to the other two samples, highlighting that the integration of the NiCoFe alloy onto graphite foil has granted an additional shielding effectiveness. The enhancement in SE_T of graphite after NiCoFe deposition could mostly be attributed to the increased absorption loss (SE_A) (Fig. 3c). The average SE_A values were 42.15 dB for the graphite foil, 35.35 dB for the free-standing NiCoFe film, and 54.82 dB for the NiCoFe/graphite composite. The average reflection loss (SE_R) values were 12.35 dB, 15.07 dB, and 14.08 dB for graphite, free-standing NiCoFe film, and NiCoFe/graphite, respectively, indicating that the

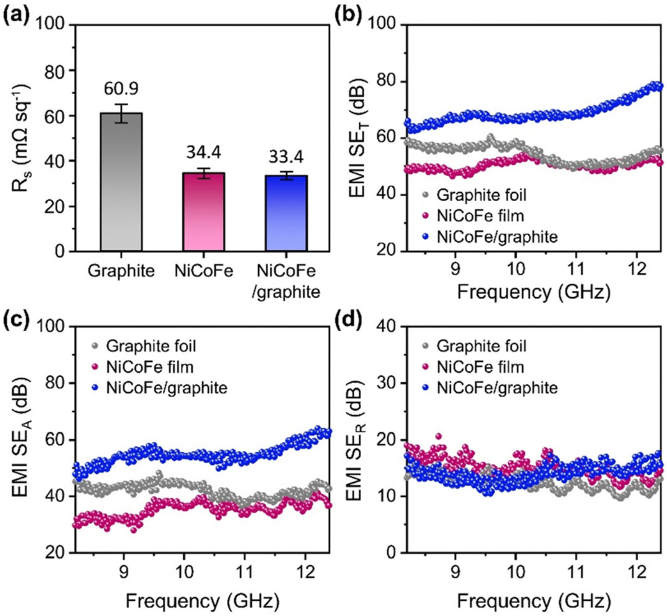

Fig. 3 EMI shielding performance of NiCoFe/graphite composite for X-band EM waves. (a) Sheet resistance of the graphite foil, NiCoFe alloy film, and NiCoFe/graphite composite. (b)–(d) EMI shielding effectiveness of the graphite foil, NiCoFe alloy film, and NiCoFe/graphite composite: (b) total shielding effectiveness, (c) absorption loss, and (d) reflection loss.

presence of NiCoFe film also enhanced SE_R due to the higher conductivity of NiCoFe than that of graphite. Because the EMI shielding effectiveness depends critically on the thickness of the shielding material (SE_A scales with the thickness although SE_R is mostly constant), we also evaluated the shielding effective normalized by the thickness. Specifically, we compared the absolute shielding effectiveness (SSE/t) of the samples, which were obtained by dividing the measured shielding effectiveness by the thickness and density (Fig. S5, ESI†). The NiCoFe/graphite composite exhibited higher SSE/t values compared to the pristine graphite foil in the X-band regime, further confirming the advantage of introducing the NiCoFe alloy film for enhancing the EMI shielding performance. Although the free-standing NiCoFe film outperforms the NiCoFe/graphite composite in terms of SSE/t, combining the NiCoFe alloy with graphite foil is more practical because producing NiCoFe films at thicknesses comparable to graphite for use as a stand-alone shielding material is challenging and cost-prohibitive. The total shielding effectiveness of the NiCoFe/graphite composite can further be enhanced by increasing the thickness of the NiCoFe film (Fig. S6, ESI†).

For the characterization of the shielding performance against magnetic-field-dominant ELF EM waves, we applied a uniform AC magnetic field (60 Hz) on the shield using a Helmholtz coil and measured the reduction in the magnetic field compared to the initial field (Experimental section in ESI†) (Fig. 4a). We tested 60 Hz in our study because this is the standard frequency for alternating current in electrical power supply systems and electronic devices in North America and many other parts of the world.[36,37] In addition, magnetic properties of the graphite foil and free-standing NiCoFe film were also characterized to analyze the effect of the NiCoFe film on ELF magnetic field shielding in more detail (Fig. 4b and c). The saturation magnetization (M_S) of the NiCoFe film was 112.1 emu g^{-1}, which was higher than that of Ni (56.3 emu g^{-1}) but lower than that of Co (164.2 emu g^{-1}) (Fig. 4d). Notably, M_S of NiCoFe exceeds the value predicted from the rule of mixture for 2 : 1 Ni/Co alloy (92.3 emu g^{-1}), indicating that the addition of Fe (221.8 emu g^{-1}) increased M_S of NiCoFe compared to NiCo (Fig. S7, ESI†).[38] NiCoFe also showed much lower coercivity (16.6 Oe) compared to Ni (52.2 Oe) and Co (117.8 Oe) (Fig. 4e), highlighting that the NiCoFe film can be easily magnetized to serve as a shield against ELF magnetic fields. Although Fe exhibited magnetic properties more suited for magnetic field shielding (higher M_S and lower coercivity), the stability of the NiCoFe ternary alloy against oxidation compared to Fe motivates the practical use of the NiCoFe film for EMI shielding. Fig. 4f shows the SE and shielding rate of the NiCoFe/graphite composite, which was calculated based on the following equation.

$$\text{Shielding rate}\,(\%) = \frac{B_\mathrm{i} - B_\mathrm{s}}{B_\mathrm{i}} \times 100(\%) \qquad (6)$$

where B_i is the initial magnetic field and B_s is the magnetic field after shielding. The gradual increase in shielding effectiveness and shielding rate with increasing thickness of the NiCoFe film was verified. The composite shield exhibited SE of 0.35 dB and shielding rate of 4% for the NiCoFe thickness of ~17 μm, which increased to 4.53 dB and 40.6% when the NiCoFe thickness increased to ~950 μm. The demonstration of ELF magnetic field shielding properties confirms that the NiCoFe/graphite composite can achieve effective shielding against EM waves in multiple

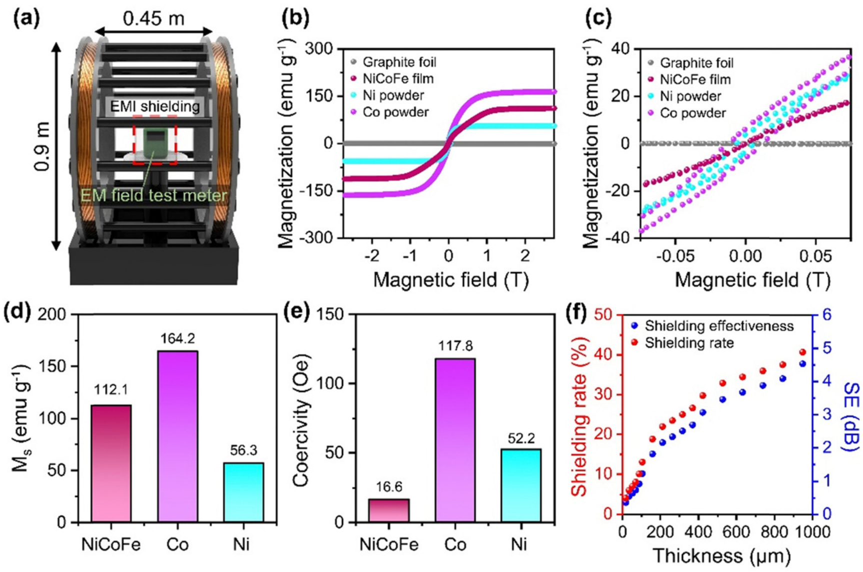

Fig. 4 EMI shielding performance of NiCoFe/graphite composite for extremely-low-frequency magnetic fields. (a) Scheme describing the Helmholtz coil and shielding box set-up for characterization of ELF magnetic field shielding performance. (b) and (c) M–H curves of the graphite foil and NiCoFe alloy film, along with those of Ni and Co powders. Panel (c) displays a narrower magnetic field region centered around 0 T of panel (b). (d) and (e) Magnetic properties of the NiCoFe alloy film, along with Co and Ni powders: (d) saturation magnetization and (e) coercivity. (f) Thickness dependence of the EMI shielding performance of the NiCoFe/graphite composite against 60-Hz magnetic fields.

frequency ranges owing to synergistic effects from the constituent graphite and NiCoFe.

Thermal conductivity

For practical applications, EMI shielding films with high thermal conductivity are highly desired for effectively dissipating heat from the protected system to the surrounding.[39] To investigate the effect of NiCoFe deposition on thermal management capability of the graphite foil, we determined the thermal conductivity based on the following relation:

$$k = \alpha C_{\mathrm{p}}\rho \tag{7}$$

where k is the thermal conductivity, α is the thermal diffusivity, C_{p} is the specific heat capacity and ρ is the density. We first measured the thermal diffusivities (Fig. S8a, ESI†) and specific heat capacities (Fig. S8b, ESI†) of the samples. We found that the introduction of NiCoFe film increased both the thermal diffusivity and specific heat capacity of the graphite foil, with the thermal diffusivity increasing from 2.31 $\mathrm{mm^2\ s^{-1}}$ to 4.09 $\mathrm{mm^2\ s^{-1}}$ and the specific heat capacity increasing from 0.67 $\mathrm{J\ g^{-1}\ K^{-1}}$ to 0.73 $\mathrm{J\ g^{-1}\ K^{-1}}$. The density of the NiCoFe-deposited graphite foil was slightly smaller (1.04 $\mathrm{g\ cm^{-3}}$) than that of the pristine counterpart (1.16 $\mathrm{g\ cm^{-3}}$) (Fig. S8c, ESI†). The smaller density of NiCoFe/graphite composite is attributed to the out-of-plane expansion ($\sim$30%) of the graphite foil due to intercalation of metal ions during electrodeposition, which offsets the effect of the NiCoFe film in increasing density (Fig. S9, ESI†). Because of the enhanced thermal diffusivity and specific heat capacity, the thermal conductivity was increased by 72% from 1.80 $\mathrm{W\ m^{-1}\ K^{-1}}$ to 3.09 $\mathrm{W\ m^{-1}\ K^{-1}}$ after electrochemical deposition (Fig. S8d, ESI†). This increase can be attributed to the higher thermal conductivity of NiCoFe compared to graphite (especially, the effects of cobalt and nickel were significant). These results indicate that the NiCoFe-coated graphite foil is a better shielding material than a pristine graphite foil in terms of the thermal management capability.

Mechanical properties

The shielding materials also require good mechanical properties for broad applications.[40] Elastic modulus and ultimate strength were measured to evaluate the mechanical properties of the shield. The elastic modulus and ultimate strength were significantly increased when the graphite foil was deposited with the NiCoFe film (Fig. S10, ESI†). In particular, the elastic moduli of pristine and NiCoFe-deposited graphite foils were 2.24 MPa and 29.95 MPa, respectively (Fig. S10a, ESI†). Similarly, the ultimate strength was much higher for NiCoFe-coated graphite foil (36.65 MPa) compared to the pristine counterpart (4.50 MPa) (Fig. S10b, ESI†). Comparison between the mechanical properties of samples suggests that the NiCoFe coating not only enhances the EMI shielding performance, but also improves mechanical robustness of the graphite foil.

Conclusions

In summary, we developed an EMI shield effective for X-band and extremely low frequencies by integrating electrically conductive graphite foil and magnetically permeable NiCoFe alloy film into a composite. In addition to shielding against extremely low-frequency EM waves by shunting magnetic flux, the NiCoFe layer enhanced the conductivity of the graphite foil to further enhance the shielding effectiveness in high-frequency regime. Meanwhile, through successful development of a metal composition with extremely low magnetic resistance, we achieved a nearly 40% shielding effectiveness for extremely low-frequency EM waves, even with thicknesses on the order of several hundred micrometers. Considering the lack of research on shielding materials in the low-frequency and extremely low-frequency ranges, our efforts hold the potential to address remaining risks still closely embedded in our daily lives, particularly associated with elements like underground power transmission lines.[41] Given the continued influence of these elements, our study provides a tangible and promising avenue towards resolving these issues.

Author contributions

J. K., D. C., and S.-W. K. initiated and supervised all the research. J. L., Y. S. C., and D. R. designed and pursued the experimental works and data analysis. H. K., S. J., D. L., J. W. H., M. C., J. H. S., J.-Y. S., and I. S. K. assisted additional data collection and analysis. The manuscript was written through contributions of all authors. All authors have given approval to the final version of the manuscript.

Data availability

The data supporting this article have been included as part of the ESI.† Also, the data can be provided from the corresponding authors upon reasonable requests.

Conflicts of interest

There are no conflicts of interest to declare.

Acknowledgements

This research was funded by Korea Electric Power Corporation (No. R21XA02). This work was also partially supported by a National Research Foundation of Korea (NRF) grant funded by the Korean Government (MSIT) (RS-2023-00208538) and the Korea Basic Science Institute (KBSI) National Research Facilities and Equipment Center (NFEC) grant funded by the Korean Government (Ministry of Education) (2019R1A6C1010031).

References

1 T. Alsop, Number of Wireless Local Area Network (Wlan) Connected Devices Worldwide from 2016 to 2021 (in Billions),

https://www.statista.com/statistics/802706/world-wlan-connected-device/, (accessed 09 Dec, 2023).
2 D. D. L. Chung, *Mater. Chem. Phys.*, 2020, **255**, 123587.
3 R. Baan, Y. Grosse, B. Lauby-Secretan, F. El Ghissassi, V. Bouvard, L. Benbrahim-Tallaa, N. Guha, F. Islami, L. Galichet and K. Straif, *Lancet Oncol.*, 2011, **12**, 624–626.
4 L. Liu, H. Deng, X. Tang, Y. Lu, J. Zhou, X. Wang, Y. Zhao, B. Huang and Y. Shi, *Proc. Natl. Acad. Sci. U. S. A.*, 2021, **118**, e2105838118.
5 J. R. Jauchem, *Int. Arch. Occup. Environ. Health*, 1997, **70**, 9–21.
6 A. Iqbal, P. Sambyal and C. M. Koo, *Adv. Funct. Mater.*, 2020, **30**, 2000883.
7 T. K. Gupta, B. P. Singh, S. R. Dhakate, V. N. Singh and R. B. Mathur, *J. Mater. Chem. A*, 2013, **1**, 9138–9149.
8 L.-C. Jia, D.-X. Yan, C.-H. Cui, X. Jiang, X. Ji and Z.-M. Li, *J. Mater. Chem. C*, 2015, **3**, 9369–9378.
9 C. R. Paul, R. C. Scully and M. A. Steffka, *Introduction to electromagnetic compatibility*, John Wiley & Sons, 2022.
10 J. Zhang, J. Li, G. Tan, R. Hu, J. Wang, C. Chang and X. Wang, *ACS Appl. Mater. Interfaces*, 2017, **9**, 42192–42199.
11 F. Shahzad, M. Alhabeb, C. B. Hatter, B. Anasori, S. Man Hong, C. M. Koo and Y. Gogotsi, *Science*, 2016, **353**, 1137–1140.
12 A. Iqbal, F. Shahzad, K. Hantanasirisakul, M.-K. Kim, J. Kwon, J. Hong, H. Kim, D. Kim, Y. Gogotsi and C. M. Koo, *Science*, 2020, **369**, 446–450.
13 Z. Gao, A. Iqbal, T. Hassan, S. Hui, H. Wu and C. M. Koo, *Adv. Mater.*, 2024, 2311411.
14 A. Iqbal, T. Hassan, S. M. Naqvi, Y. Gogotsi and C. M. Koo, *Nat. Rev. Electr. Eng.*, 2024, **1**, 180–198.
15 N. Yousefi, X. Sun, X. Lin, X. Shen, J. Jia, B. Zhang, B. Tang, M. Chan and J.-K. Kim, *Adv. Mater.*, 2014, **26**, 5480–5487.
16 W. Ren, Y. Yang, J. Yang, H. Duan, G. Zhao and Y. Liu, *Chem. Eng. J.*, 2021, **415**, 129052.
17 S. Gupta and N.-H. Tai, *Carbon*, 2019, **152**, 159–187.
18 X. Luo and D. D. L. Chung, *Composites, Part B*, 1999, **30**, 227–231.
19 Y. Yang, M. C. Gupta, K. L. Dudley and R. W. Lawrence, *Nano Lett.*, 2005, **5**, 2131–2134.
20 J. Liang, Y. Wang, Y. Huang, Y. Ma, Z. Liu, J. Cai, C. Zhang, H. Gao and Y. Chen, *Carbon*, 2009, **47**, 922–925.
21 R. B. Keller, *Design for Electromagnetic Compatibility--In a Nutshell: Theory and Practice*, ed. R. B. Keller, Springer International Publishing, Cham, 2023, pp. 95–109, DOI: 10.1007/978-3-031-14186-7_8.
22 X. Xu, W. Liu, Y. Huang, W. Li and S. Che, *J. Magn. Magn. Mater.*, 2023, **570**, 170509.
23 Y. Xia, W. Gao and C. Gao, *Adv. Funct. Mater.*, 2022, **32**, 2204591.
24 S. Geetha, K. K. Satheesh Kumar, C. R. K. Rao, M. Vijayan and D. C. Trivedi, *J. Appl. Polym. Sci.*, 2009, **112**, 2073–2086.
25 M. H. Al-Saleh and U. Sundararaj, *Carbon*, 2009, **47**, 1738–1746.
26 R. G. Olsen and P. Moreno, *IEEE Trans. Electromagn. Compat.*, 1996, **38**, 460–468.
27 A. Canova, J. C. del-Pino-López, L. Giaccone and M. Manca, *IEEE Trans. Magn.*, 2015, **51**, 1–4.
28 Y. S. Cho, D. Rhee, J. Eom, J. Kim, M. Jung, Y. Son, Y.-K. Han, K. K. Kim and J. Kang, *Small Sci.*, 2022, **2**, 2200043.
29 S. Hassani, K. Raeissi and M. A. Golozar, *J. Appl. Electrochem.*, 2008, **38**, 689–694.
30 N. P. Wasekar, P. Haridoss, S. K. Seshadri and G. Sundararajan, *Surf. Coat. Technol.*, 2016, **291**, 130–140.
31 G. Barati Darband, M. Aliofkhazraei and A. S. Rouhaghdam, *J. Colloid Interface Sci.*, 2019, **547**, 407–420.
32 C. T. J. Low, R. G. A. Wills and F. C. Walsh, *Surf. Coat. Int.*, 2006, **201**, 371–383.
33 W.-S. Chang, Y. Wei, J.-M. Guo and F.-J. He, *Open J. Met.*, 2012, **2**, 18–23.
34 M. Zhang, Y. Liu, B. Liu, Z. Chen, H. Xu and K. Yan, *ACS Catal.*, 2020, **10**, 5179–5189.
35 S. Budi, B. Kurniawan, D. M. Mott, S. Maenosono, A. A. Umar and A. Manaf, *Thin Solid Films*, 2017, **642**, 51–57.
36 B.-C. Lee, H.-M. Johng, J.-K. Lim, J. H. Jeong, K. Y. Baik, T. J. Nam, J. H. Lee, J. Kim, U. D. Sohn, G. Yoon, S. Shin and K.-S. Soh, *J. Photochem. Photobiol., B*, 2004, **73**, 43–48.
37 A. Legros, J. Modolo, S. Brown, J. Roberston and A. W. Thomas, *PLoS One*, 2015, **10**, e0132024.
38 G. Shamsutdinov, P. Zhao, S. Bhattiprolu, J.-C. Zhao and B. Nadgorny, *Sci. Rep.*, 2022, **12**, 1957.
39 H. Zhao, J. Yun, Y. Zhang, K. Ruan, Y. Huang, Y. Zheng, L. Chen and J. Gu, *ACS Appl. Mater. Interfaces.*, 2022, **14**, 3233–3243.
40 J. Cheng, C. Li, Y. Xiong, H. Zhang, H. Raza, S. Ullah, J. Wu, G. Zheng, Q. Cao, D. Zhang, Q. Zheng and R. Che, *Nanomicro Lett.*, 2022, **14**, 80.
41 Z. H. Zhou and G. H. Chen, *Proc. Eng.*, 2015, **130**, 1503–1513.